J. Electrochem. Sci. Eng. **12(3)** (2022) 485-499; http://dx.doi.org/10.5599/jese.1224

Open Access : : ISSN 1847-9286

www.jESE-online.org

Original scientific paper

Supercapacitor performance gains from structural modification of carbon electrodes using gamma radiations

Norliyana Mustapar, Mohd Amir Radhi Othman✉, Mohd Sukor Su'ait[1], Mohd Suleman[2], Wai Yin Wong[3] and Kee Shyuan Loh[3]

Department of Applied Physics, Faculty of Science and Technology, Universiti Kebangsaan Malaysia, 43600 UKM Bangi, Selangor, Malaysia

[1]Solar Energy Research Institute (SERI), Universiti Kebangsaan Malaysia, 43600 UKM Bangi, Selangor, Malaysia

[2]Shibli National College, Veer Bahadur Singh Purvanchal University, Uttar Pradesh 222003, India

[3]Fuel Cell Institute, Universiti Kebangsaan Malaysia, 43600 UKM Bangi, Selangor, Malaysia

Corresponding author: ✉maro@ukm.edu.my; Tel.: +603-8921-3474; Fax: +603-8921-3777

Received: December 31, 2021; Accepted: February 16, 2022; Published: March 10, 2022

Abstract

The performance of supercapacitors (SC) strongly depends on how their activated carbon (AC) electrodes were synthesized from precursor materials and pretreatments applied to them. This study investigates the effect of direct and filtered gamma radiations applied as pretreatments to the AC. The exposure doses used were from 0.1 kGy to 6 kGy. The high gamma-energy and high dose of the pretreatment broke the randomly orientated graphitic crystal lattices inside AC particles and disturbed the existing functional group populations. The filtered radiation pretreatment at 1 kGy, which contains a higher composition of secondary electrons than direct radiation pretreatment, yields AC with the best overall SC performance. The SC cell made from 1 kGy filtered radiation pretreatment AC showed higher specific capacitance 73.1 % (218.58 F g^{-1}), specific energy 73.54 % (10.96 W h kg^{-1}) and specific power of 8.36 % (155.67 W kg^{-1}) compared to the sample without any radiation pretreatment. This study explicitly shows the benefit of secondary electrons in the radiation field, which produce decisively defect sites on the AC lattices for gains in SC performance.

Keywords

Supercapacitor cell; activated carbon; gamma pretreatment; secondary electrons radiation

Introduction

An economic development based on non-renewable energy sources is unsustainable. Unfortunately, such energy sources significantly influence the energy consumption in the world today as the demand for energy keeps increasing. Therefore, renewable and green energy sources are attracting current energy research to reduce the dependence on unsustainable energy sources [1]. In the ecosystem of renewable and green energy sources, supercapacitor (SC), also known as ultracapacitor,

is a promising green energy storage device. SC is an ideal electrical energy storage device with moderate energy capacity and high-power delivery [2], long life cycle [3], low maintenance [4], desirable safety and fast dynamics of charge propagation compared to conventional energy storage devices. Due to such benefits, SCs are used primarily in hybrid electric vehicles, electric vehicles, fuel cell vehicles such as passenger cars, trains and trolleybuses [5].

The electrode material is one of the major components that determine the performance of SC. The commonly used electrode materials are based on carbonaceous materials such as carbon nanotubes [6], carbon nanofibers [7], carbon aerogel [8], graphene [9], and activated carbon (AC) [10]. The non-carbon-based materials (found in pseudocapacitors) include conducting polymers [11], and transition metals oxides such as NiO [12], RuO_2 [13], IrO_2 [14], and MnO_2 [15]. However, AC is the most widely studied electrode material due to its high porosity structure, high surface area, endurance, non-toxicity and potential to alleviate agro-industrial wastes [16]. The precursor materials of AC are naturally obtained from agricultural wastes, such as coconut shells [17], oil palm empty fruit bunches [18], cassava peel [19], banana fibers [20], jackfruit peels [21], sunflower seed shells [22], bamboos [23], rice straw [24], durian shells [25], and coffee beans [26] due to their low cost and abundant availability.

The modification methods involved during the precursor preparation play an essential role in producing desired carbon electrode properties [27]. Generally, the carbonization (in an inert gas at high temperature) and activation (physical or chemical) methods are used separately or in combinations to modify the AC electrode pore structure, surface area, and conductivity. However, the SC incorporating AC electrodes from biomass precursor has reached the limit of useable surface area for electrochemical performance gains. It has been reported that the performance of such SCs does not linearly increase with the increase in surface area due to non-ideal pore size distribution [28]. Thus, further viable treatment on the AC should focus on modifying carbon lattices and functional group populations. Typically, functional groups present in AC from biomass precursors (coconut shell [29]) are associated with O-H bonds of hydroxyl groups, C-H bonds of methyl groups and C=C bonds.

Gamma radiation on carbonaceous materials has long been attributed to improving structural modifications in terms of the material disorder [30], increased pore width, and mesopore formation, contributing to a broader distribution of pore sizes [31]. Hence, prior application of radiation treatment on the AC powder led to better SC performance [32]. However, most gamma energy does not deposit onto the AC powder during stochastic interactions (for uncharged particles such as photons) under direct gamma radiation. Instead, the energy is carried away by scattering the knocked-out secondary electrons. This effect intensifies for 1.25 MeV-photon when the Compton scattering interaction dominates, resulting in more energetic and long-range secondary electrons scattering. Another issue is that AC materials have a low interaction cross-section with photons at the energy of 1.25 MeV. The solution to these problems is to place a metallic layer as a filter (radiation attenuator) between the radiation source and AC powder, which acts as an additional interaction site for producing secondary electrons. The secondary electrons created from the metallic layer will reach the AC powder and interact deterministically (for charged particles such as energetic electrons) to create typical lattice defects, such as Stone-Wales defects and vacancy defects [33]. The defects created can influence the electrochemical property of carbonaceous materials [34].

This study used gamma treatment from a Co-60 source with increasing doses between 0.1 and 6 kGy to radiate the AC commercial (ACC) powder. The ACC was exposed directly to gamma radiation (direct radiation), or the ACC was placed inside a copper envelope before radiation (filtered radiation). This study investigates the microscopic impact of the radiation modalities on the ACC

properties, such as pore networks, surface morphology, chemical bonds, and lattices. Finally, the effect of the radiation modalities on electrochemical performance was investigated by using the ACC as SC electrodes. We elucidated and differentiated the effect of the radiation modalities in producing radiation defects in the ACC from the physical and electrochemical analyses.

Experimental

Powder irradiation setups

A plastic bag filled with 0.5 g of ACC powder (Bravo green Sdn Bhd) was placed inside a revolving container (Gammacell 220 Excel) (Figure 1A) in the direct radiation modality with a Co-60 source (1.25 MeV-photon). Another plastic bag was enclosed in a copper foil envelope of 0.13 mm-thick-layer in the filtered radiation modality (Figure 1A inset). The irradiation doses used were 0.1, 0.5, 1.0, 3.0, and 6.0 kGy for each radiation modality (the samples from direct radiation were denoted as ACCD-0.1, ACCD-0.5, ACCD-01, ACCD-03, and ACCD-06, respectively, and filtered radiation samples as ACCF-0.1, ACCF-0.5, ACCF-01, ACCF-03, and ACCF-06, respectively). Figure 1B shows a schematic representation of gamma radiation on the samples.

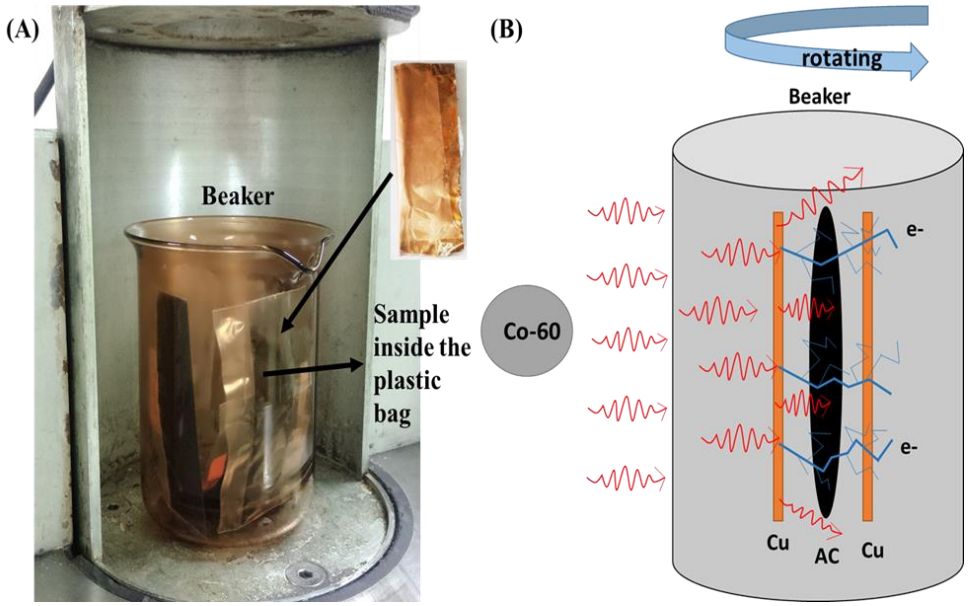

Figure 1. *(A) ACC powder in a plastic bag ready for exposure to direct gamma radiation in the Gammacell 220 Excel. The plastic bag is enclosed with copper foil in the filtered radiation modality. (B) Schematic representation of gamma radiation on the samples, where copper foil attenuates the primary radiation (curly red arrow) and produces secondary electrons, e^- (blue tracks). The copper foil is absent in the direct radiation, leaving mostly direct gamma interaction with ACC powder*

Preparation of supercapacitor cells

The irradiated ACC powders were further grounded and sieved (Lab. Tes Sieve BS 140) until an average particle size less than 53 μm was obtained. The electrodes were prepared by mixing 90 wt.% ACC powder, 5 wt.% carbon black (Sigma-Aldrich) and 5 wt.% PVDF-HFP (Sigma-Aldrich) to form a slurry at room temperature. The slurry was brush-painted on graphite tape (commercially available-Ziqrah Scientific) with 1 cm^2 of the cut area. The mass loading of active materials is about ~4.2 mg on the electrode after drying. Then, two symmetric electrodes were soaked in 6 M KOH electrolyte before being made up into SC cell by sandwiching a polypropylene separator (25 µm thick, Celgard 3501).

Physical characterizations

Field emission scanning electron microscope (FESEM, Merlin, Zeiss 2013) was used to observe ACC, ACCD and ACCF powders morphologies. Micrometric ASAP 2010 instrument using liquid nitrogen adsorbate at 77 K was used to determine the sample BET specific surface area (S_{BET}) and pore distribution parameters such as micropore surface area (S_{micro}), mesopore surface area (S_{meso}), micropore volume (V_{micro}), mesopore volume (V_{meso}) and average pore diameter (D_p).

X-ray diffraction (XRD) patterns of ACC, ACCD and ACCF samples were determined by X-ray diffractometer (Bruker AXS: model D8 Advance) with CuK$_\alpha$ radiation (λ= 0.154 nm). The interplanar spacing (d_{002} and d_{100}) for all ACCs powder was determined from equation (1) [35]:

$$d = \frac{\lambda}{2}\sin\theta \quad (1)$$

where λ is the wavelength of the X-ray, and θ is the reflection at angles θ_{002} and θ_{100} for peaks (002) and (100), respectively. The layer stacking height (L_c) from the (002) peak and longitudinal size of stack width (L_a) from the (100) peak were calculated from the Debye- Scherrer equations (2) and (3) [35]:

$$L_c = 0.9\left(\frac{\lambda}{\beta_{002}\cos\theta_{002}}\right) \quad (2)$$

$$L_a = 1.84\left(\frac{\lambda}{\beta_{100}\cos\theta_{100}}\right) \quad (3)$$

where β_{002} and β_{100} is the full width at half maximum of the symmetrically shaped diffraction peaks of (002) and (100) planes, while θ_{002} and θ_{100} are (002) plane and (100) plane reflection angles, respectively.

Raman spectra were recorded from 650 to 4000 cm^{-1} using a 514 nm laser beam for selected samples (Thermo Scientific I Model (DXR2xi)). The chemical structure of the selected samples was studied using Fourier transform infrared spectroscopy (FTIR, Perkin Elmer Spectrum 400 FT-IR).

Electrochemical characterizations

Electrochemical performance of SC (two-electrode configuration) made from ACC, ACCD and ACCF electrodes were investigated. In electrochemical impedance spectroscopy, EIS (Metrohm Autolab B.V), measurements were carried out using 10 mV amplitude in a frequency range from 1 MHz to 0.01 Hz. From EIS data, the specific capacitance (C_{sp}) of the SC with two equal electrodes was calculated using equation (4):

$$C_{sp} = -\frac{1}{\pi f_1 Z''_1 m} \quad (4)$$

where f_1 is the lowest frequency of measurement, Z'' is the imaginary impedance value (Ω) at f_1, and m is the total mass of active material (g) of two electrodes.

The SC charge storage capacity was studied using cyclic voltammetry, CV (Metrohm Autolab B.V) and C_{sp} for CV were calculated for two electrodes using equation (5) [36]:

$$C_{sp} = \frac{1}{2mv(\Delta V)}\left(\int_{V_1}^{V_2} i(V)\mathrm{d}V\right) \quad (5)$$

where v (mV s^{-1}) is the scan rate, ΔV (V) is the potential window, while $\int i(V)\mathrm{d}V$ is the total voltammetric charge bounded by the negative and positive sweeps (the area inside the CV curve).

Galvanostatic charge-discharge, GCD (5 V, 10 mA NEWARE BTS 3000 battery testing system) analysis was performed to produce C_{sp}, specific power (P) and specific energy (E) of the two electrodes SC based on equations (6) [37], and (7 and 8) [38]:

$$C_{sp} = \frac{2i}{\left(\frac{\Delta V}{\Delta t}\right)m} \quad (6)$$

$$P = \frac{Vi}{m} \quad (7)$$

$$E = \frac{Vit}{m} \quad (8)$$

where i is the discharge current, ΔV is the total potential difference during a complete discharge process, Δt is the time for complete discharge, V is the cell operational voltage window, and t is discharging time (s).

Results and discussion

Physical characterizations

Selected ACC samples were chosen based on the results of their SC electrochemical performance obtained earlier. In the FESEM and N_2 adsorption-desorption analysis, the selected samples include non-radiated and radiated samples of 0.5 and 1.0 kGy. In structural-sensitive characterizations such as XRD, Raman spectroscopy and FTIR analysis, the 6.0 kGy radiated samples were also included.

FESEM micrographs

FESEM characterization of surface morphologies of the selected samples shows that the ACC naturally exhibited a porous texture with a network of open pores, as shown in Figure 2. This richness of pore sizes in the samples is beneficial for SC electrodes as it provides good ionic transportation [39]. The electrode pores developed during the activation process result from the breakdown of the biomass precursor structure [40].

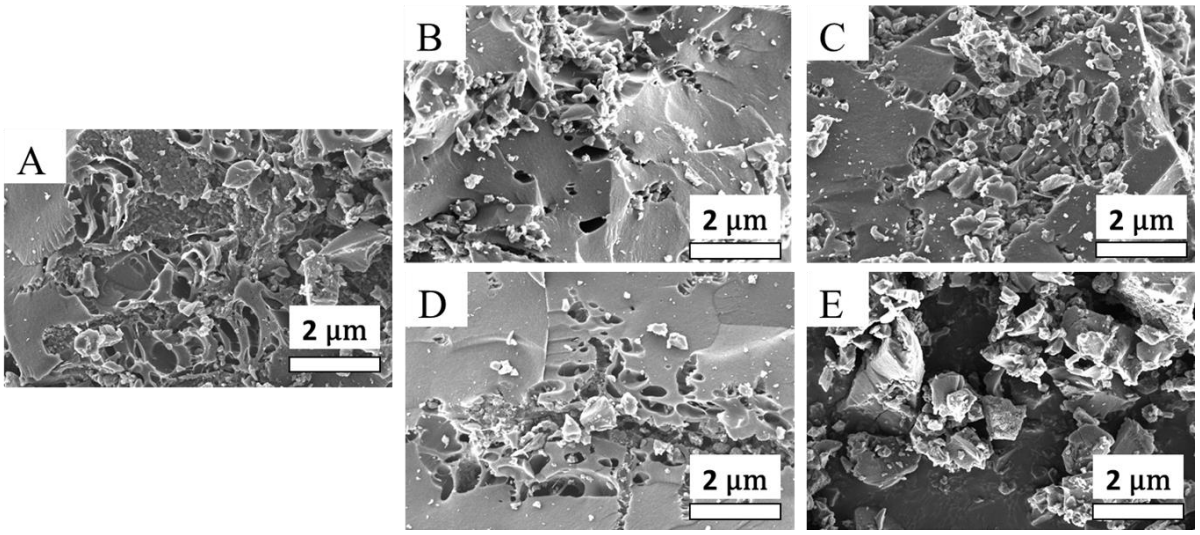

Figure 2. *FESEM micrographs for: (A) ACC-00 with complex open pores network; (B) ACCD-0.5 with surface roughness and some pores network extending deep into the particle; (C) ACCD-01 open pores network filled with smaller particles; (D) ACCF-0.5 same as (A); (E) ACCF-01 with granulation of smaller particles on the surface*

The morphological effect due to radiation exposures is not directly discernible through the FESEM. However, the FESEM does show that the distribution of granulations and the surface roughness of the samples are almost identical. The network of pores was confirmed through N_2 adsorption-desorption analysis.

N_2 adsorption-desorption

The influence of gamma radiations on the porous texture of ACC was captured in N_2 adsorption-desorption measurements (Figure 3). The N_2 adsorption-desorption isotherms of the selected samples show that the overall shapes are typical adsorption-desorption curves for AC materials [41]. The samples IUPAC curve classification is a combination of type I and type IV isotherms [42]. Type I isotherm is characteristic of microporous samples [43], while type IV isotherm indicates the presence of mesopores [44]. The values of the pore structure parameters (Table 1) from the adsorption isotherms showed a general trend which suggests that radiation exposures cause surface area to slightly decrease for radiated samples, compared to the non-irradiated sample [31]. However, the ACCF-01 sample has the most significant volume of $S_{meso,}$ which is essential for electrolyte ions transport [45] into micropore surfaces and improves power performance at high current densities.

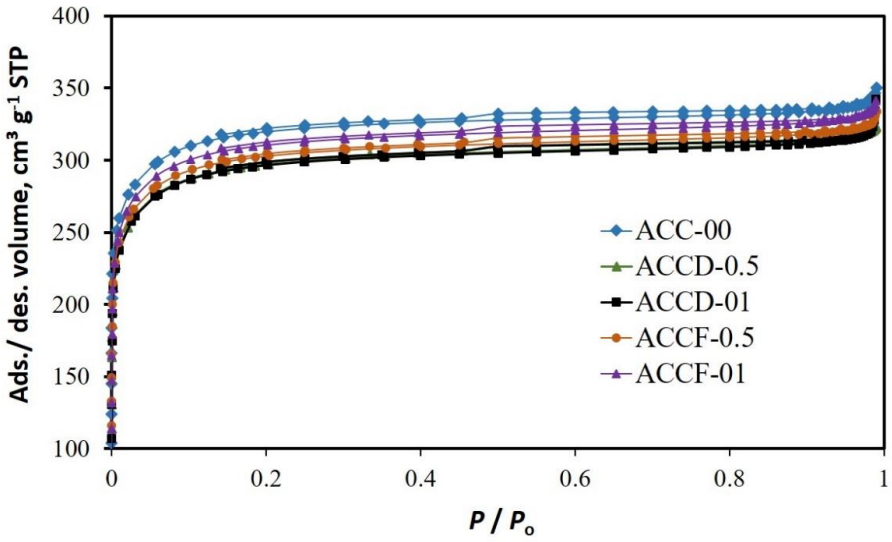

Figure 3. *Nitrogen adsorption-desorption isotherms for selected ACC, ACCD and ACCF samples*

Table 1. *Pore parameters for selected ACC, ACCD and ACCF samples*

Radiation modality	Non-radiated	Direct radiation		Filtered radiation	
Radiation dose, kGy	ACC-00	ACCD-0.5	ACCD-01	ACCF-0.5	ACCF-01
S_{BET} / $m^2 g^{-1}$	1065.08	990.73	986.79	1010.07	1034.55
S_{meso} / m^2g^{-1}	214.99	215.16	212.54	214.00	221.25
S_{micro} / m^2g^{-1}	850.09	775.57	774.25	796.07	813.30
V_{meso} / cm^3g^{-1}	0.12	0.11	0.14	0.12	0.12
V_{micro} / cm^3g^{-1}	0.40	0.37	0.37	0.37	0.38
S_{meso} / S_{micro}	0.25	0.28	0.27	0.27	0.27
D_p / nm	1.99	2.00	2.01	2.00	2.00

XRD analysis

Crystallographic structures from XRD for the selected ACC powder samples are shown in Figure 4. The existence of (002) and (100) broad peaks in Figures 4(A) and 4(B) indicates that the samples are amorphous [46]. The diffraction pattern for the selected samples consists of two broad peaks, correlated with honeycomb-structure of carbon, located at around 24.6 and 43.7°, corresponding to the (002) and (100) peaks, respectively. The peak broadness represents a turbostratic or random layer lattice structure [47]. This turbostratic structure shows that the carbon layers are characterized by randomly shifted layers, unorganized stray carbons, local stacking faults, strain in the layers and varying interspacing values [48]. The structural features such as the interlayer spacings (d_{002} and d_{100}), L_c, L_a, the ratios of L_c/L_a and L_c/d_{002} of the samples calculated from equations (1)-(3) are shown in Table

2. The radiated samples interlayer spacing (d_{002} and d_{100}) values did not differ significantly from non-irradiated ones. There are significant increments of L_c and decrements of L_a from ACCD and ACCF samples, especially the ACCD-01 and ACCF-01, compared to ACC-00. The highest increment of L_c at 1 kGy dose is associated with increased intermediate carbon plane distance held by van der Waals force. This effect is attributed to the formation of defects and the appearance of intermediate dangling atoms between the carbon planes. The out-of-plane dangling atoms have a shorter distance to the next carbon plane. The decreasing of L_a at 1 kGy is due to the weakened of covalent (σ and π) bond represented by peak (100) of carbon plane [45]. Hence, the ratio of L_c/L_a and L_c/d_{002} shows the largest value for samples ACCD-01 and ACCF-01. At a higher dose (6 kGy), more defects and dangling atoms formed, causing carbon planes to collapse and break apart at the defect points. Hence, the new structures have fewer defects and the structural parameters resembling ACC-00. The increment in L_c, L_c/L_a and L_c/d_{002} values corresponds to the gain in specific capacitance of SC [49], already observed in the electrochemical characterizations section. This is due to the increase in lattice defects on ACCD and ACCF particles that indirectly affects pore distributions.

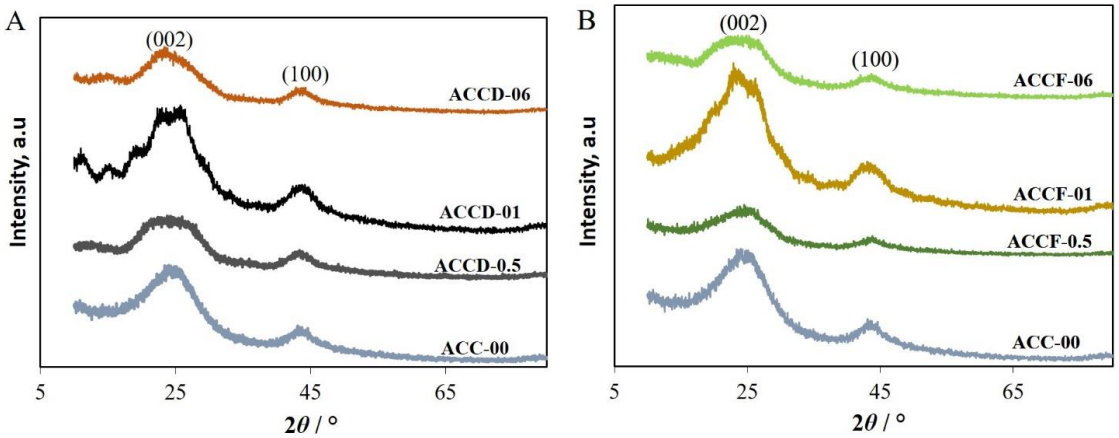

Figure 4. *XRD pattern for: (A) direct radiation modality, ACCD, and (B) filtered radiation modality, ACCF, at different irradiation doses. The non-radiated ACC-00 is shown on both sides for reference*

Table 2. *X-ray diffraction parameters for selected ACC, ACCD and ACCF samples*

ACCs	d_{002} / nm	d_{100} / nm	L_c / nm	L_a / nm	L_c / L_a	L_c / d_{002}
ACC-00	0.374	0.208	0.635	2.697	0.24	1.70
ACCD-0.5	0.370	0.208	0.713	2.481	0.29	1.92
ACCD-01	0.376	0.209	0.755	1.535	0.49	2.01
ACCD-06	0.372	0.209	0.536	2.361	0.23	1.44
ACCF-0.5	0.370	0.208	0.726	2.343	0.31	1.96
ACCF-01	0.378	0.209	0.866	1.651	0.52	2.29
ACCF-06	0.375	0.208	0.643	2.449	0.26	1.72

Raman spectroscopy

The results of Raman spectroscopy analysis performed on the selected samples are shown in Figure 5. Raman spectra consist of three prominent characteristic peaks centered around (~1340 to 1390 cm^{-1}), (~1590-1640 cm^{-1}) and (~2590-2620 cm^{-1}), corresponding to *D* band, *G* band and 2*D* bands, respectively, which is typical for AC samples [50]. The *D* band represents defect/disorder carbon. The *G* band represents the in-plane vibration of the sp^2. The 2*D* band represents graphitic carbon characteristics and its peak broadness is related to the number of carbon layers [51].

The degree of disorder of the sample is described by the intensity ratio of the *D* and *G* bands (I_D/I_G). Generally, I_D/I_G values increased after exposure to radiation, where the sample exposed to

1 kGy recorded the highest increment (Table 3). The reduction of I_D/I_G values at overdose (6 kGy) suggests that the newly formed structures break at defect points with fewer defects than the 1 kGy sample. This trend is in good agreement with the XRD analysis (L_c, L_c/L_a and L_c/d_{002}) that showed maximums at 1 kGy dose and decrements for an overdose at 6 kGy. The intensity ratio between 2D and *G* peaks (I_{2D}/I_G) indicates the number of carbon layers present in carbon material [52]. The values of I_{2D}/I_G >2, 1< I_{2D}/I_G <2, I_{2D}/I_G <1 mean the presence of single-layer graphene, bilayer graphene, and three or more layers, respectively, in the turbostratic structure of the AC [53]. Thus, Table 3 shows the presence of bilayer graphene in all AC samples.

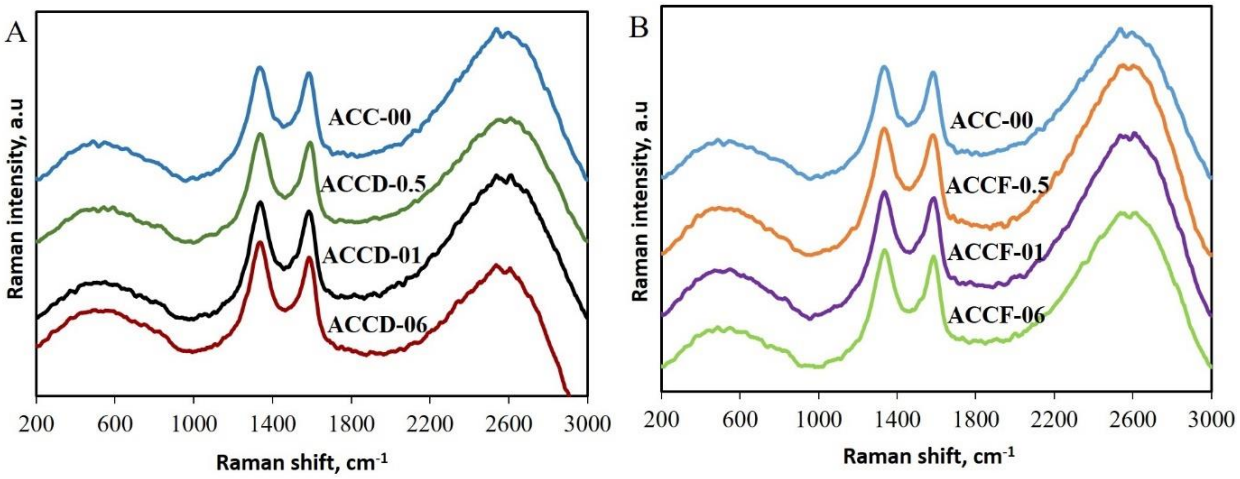

Figure 5. *Raman spectra for the selected samples: (A) direct radiation modality, ACCD, and (B) filtered radiation modality, ACCF, at different irradiation doses. The non-radiated ACC-00 is shown on both sides for reference*

Table 3. *Indicators for degree of disorder (I_D/I_G) and layers (I_{2D}/I_G)*

ACCs	I_D/I_G band	I_{2D}/I_G band
ACC-00	1.03	1.35
ACCD-0.5	1.08	1.28
ACCD-01	1.11	1.31
ACCD-06	1.09	1.16
ACCF-0.5	1.11	1.36
ACCF-01	1.12	1.40
ACCF-06	1.08	1.44

FTIR analysis

FTIR analysis is based on the characteristic transmission of reference light from the molecular bonds of functional groups present in the selected samples. The effect of gamma radiation on molecular bonds for different doses and radiation modalities can be seen clearly after normalization at a specific point (here, at 1280 cm^{-1}), as illustrated in Figure 6.

Each FTIR spectrum has a broad peak around ~3321 cm^{-1}, which is attributed to the O-H stretch of the hydroxyl functional groups [29]. The peak at ~2067 cm^{-1} is associated with the C≡C alkyne group. This peak broadness indicates that C≡C alkyne vibration becomes weaker as it was disrupted after irradiation. Three peaks observed at ~1981, ~1522 and ~1812 cm^{-1} correspond to C-H aromatic compounds, C=C aromatic compounds and C=O carbonyl compounds, respectively. The peak at ~1238 cm^{-1} is ascribed to C-O stretching, identified as lignin by Shi *et al*. [54].

In the direct radiation modality, the radiation interacts stochastically with the ACCD samples due to the material low effective atomic number ($z \approx 6$), which leads to low interaction cross-section at

1.25 MeV energy photon (carbon mass attenuation coefficient, 5.69×10^{-2} cm^2 g^{-1}) [55]. The stochastic effect is translated into interchanges of the order of FTIR lines for each identified compound peak between ACCD samples and ACC-00, Figure 6(A). The interchanges of lines show a stochastic nature that breaks the identified bonds due to direct gamma interaction with the sample carbon materials (compared to non-radiated samples). However, the secondary electrons composition is more significant in the filtered radiation modality. It is due to more secondary electrons being created (from Compton scattering) when the primary radiation gets attenuated in passing through the copper envelope. Even though the copper envelope (z = 29) has a mass attenuation coefficient of 5.26×10^{-2} cm^2 g^{-1} at 1.25 MeV-energy photon-like carbon, once the scattering of secondary electrons is created, they mostly move towards the ACCF samples. This is true given the proximity between the copper layer and ACCF and the high 1.25 MeV-energy photons involved; the ejected secondary electrons move forwards with a small scattering angle with respect to the primary photon axis. The scattered secondary electrons interact deterministically with carbon materials (as charged particles always do) and have persistent bond breakings capability. This deterministic effect can be seen in Figure 6(B), where the selected ACCF samples consistently have lesser transmittance than ACC-00 for each identified compound peak. The ACCF-01 sample has more transparency than the ACC-00 and ACCDs (Figure 6(A)) samples, suggesting that the distribution of functional groups in the ACCF-01 sample has been significantly modified.

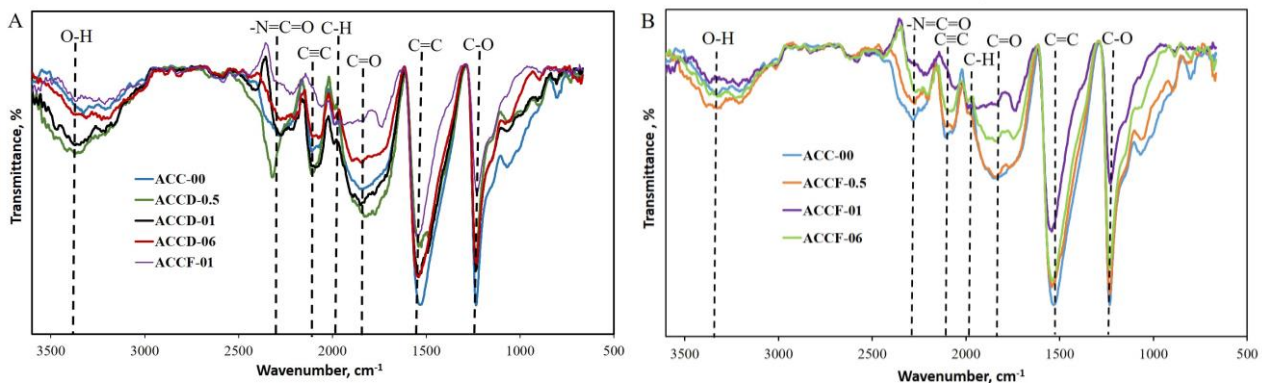

Figure 6. *FTIR spectra for the selected samples: (A) direct radiation modality, ACCD, and (B) filtered radiation modality, ACCF, at different irradiation doses. The presence of ACC-00 and ACCF-01 in both spectra is for comparison*

The reduction of C=C bonds in all radiation modalities is evident. It agrees with XRD and Raman analyses that show the increase of defects in the carbon structure due to radiation modalities. However, as shown in Figure 6(A), the effect from secondary electrons rich in filtered radiation modality (ACCF-01 sample) shows the most considerable reduction of C=C bonds.

However, an unfamiliar peak in the ACC samples appears at ~2277 cm^{-1} associated with N=C=O isocyanates. The peak appearance is believed [56] to be due to the manufacturer nitric acid treatment given to the precursor of the ACC. This peak usually appears in highly oxidized samples.

Electrochemical characterizations

Electrochemical impedance spectroscopy (EIS)

This type of electrochemical characterization investigates the favorable electrochemical properties of the ACCD and ACCF samples as SC electrodes compared to that of the ACC sample. The Nyquist plots of SC cells made from the ACCD, ACCF and ACC samples shown in Figure 7, consist of two regions with a semicircle at high frequencies and a straight-capacitive line at low frequencies.

This is a typical electric double-layer capacitance (EDLC) behavior for SC with thin electrodes [57]. The semicircle represents charge-transfer resistance, R_{ct}, due to double-layer capacitance at the interface of electrolyte/electrode and the faradaic process [16]. The semicircle intercept with Z' at high frequencies (left side) is resistance R_s, representing ionic resistance of electrolyte solution [58]. Thus, the equivalent series resistance *ESR* is given by $ESR = R_s + R_{ct}$. The EIS resistance values of the samples are listed in Table 4.

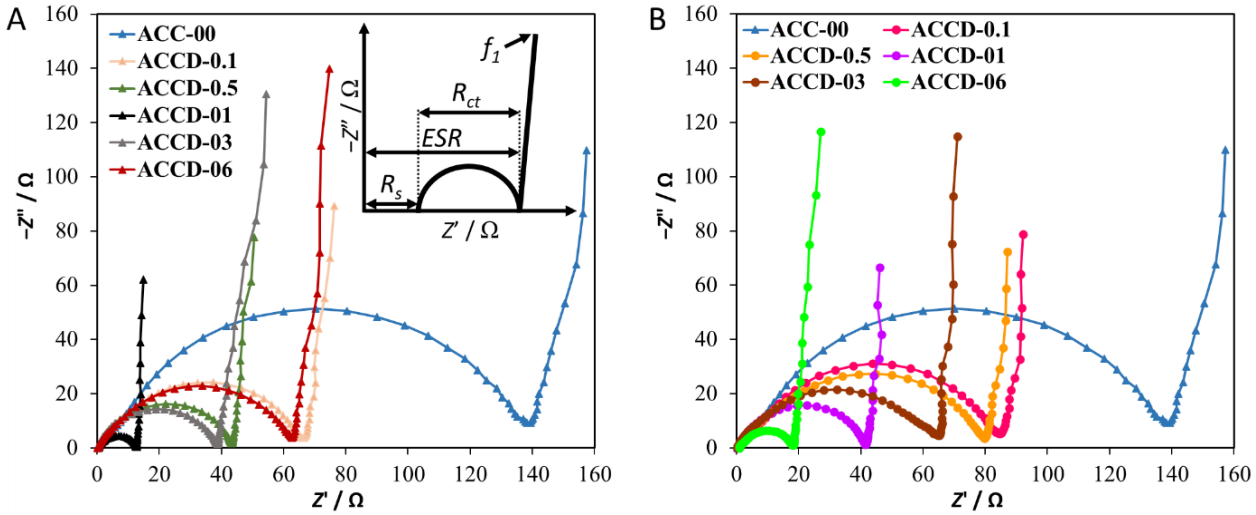

Figure 7. *Nyquist plots for SC cells made from: (A) direct radiation modality, ACCD samples, and (B) filtered radiation modality, ACCF samples, at different irradiation doses. The SC made from non-radiated ACC-00 is shown on both sides for reference. Inset of (A) shows the resistance parameters and lowest frequency point f_1 on Nyquist plot*

Interestingly, the R_{ct} values for SC cells made from ACCD and ACCF electrodes are significantly lower compared to ACC-00 SC cell and show a decreasing trend of R_{ct} and hence *ESR* values, with increasing radiation doses until 1 kGy. This is beneficial to facilitate faster ion transport across the electrode-electrolyte interface. It can be attributed to the difference in functional groups population that the ACCD and ACCF electrodes have compared to ACC-00. At overdoses of 3 and 6 kGy, the R_{ct} of ACCD SC cells starts climbing up. However, for the ACCF SC cells, R_{ct} values increase for 3 kGy but drop back at 6 kGy overdoses. The breaking apart of carbon structure at overdoses increases the R_{ct} due to an increase of contact resistance among newly formed carbon structures except for ACCF-06.

In the low-frequency region, the shorter straight-line in the Nyquist plot means a lower Z'' value at f_1, and therefore indicates an improved capacitive behavior (higher C_{sp}), as indicated by equation (4). The C_{sp} values (Table 4) show an increasing trend with irradiation doses up to 1 kGy with maximum values of 121.9 F g^{-1} (ACCD-01 electrode) and 113.9 F g^{-1} (ACCF-01 electrode), before going down due to overdose at 3 and 6 kGy.

Table 4. *Electrical parameters of SC cells*

		Non-radiated	Direct radiation					Filtered radiation				
	Parameters	ACC-00	ACCD-0.1	ACCD-0.5	ACCD-01	ACCD-03	ACCD-06	ACCF-0.1	ACCF-0.5	ACCF-01	ACCF-03	ACCF-06
EIS	R_s / Ω	0.33	0.30	0.30	0.44	0.28	0.24	0.28	0.38	0.28	0.31	0.94
	ESR / Ω	139.79	67.11	43.42	12.71	38.77	62.92	84.44	79.83	41.46	65.36	18.13
	R_{ct} / Ω	139.46	66.81	43.12	12.27	38.49	62.68	84.16	79.45	41.18	65.05	17.19
	C_{sp} / F g^{-1}	68.95	84.84	97.42	121.90	58.03	54.22	96.03	104.85	113.92	65.99	64.94
CV	C_{sp} / F g^{-1}	66.23	82.80	92.40	104.31	81.82	81.41	88.99	95.39	116.73	86.52	84.30
GCD	C_{sp} / F g^{-1}	58.80	85.95	96.04	107.18	61.13	53.23	91.49	98.87	218.58	73.28	71.99
	P / W kg^{-1}	142.65	142.97	144.87	153.5	145.33	136.4	146.12	147.57	155.67	143.22	136.71
	E / Wh kg^{-1}	2.90	4.30	4.88	5.84	3.12	2.51	4.73	5.24	10.96	3.69	3.53

Cyclic voltammetry (CV)

CV measurements were conducted within a potential window from 0 to 1 V and scan rates of 1 mV s^{-1}. Figure 8 shows that all SC cells have similar rectangular shapes, typical for an electrical double layer SC [59]. The capacitive performance (C_{sp} values were calculated using equation (5)) is dependent on irradiation doses and radiation modalities applied on the AC powder. The area of the CV-curve that determines the SC cells performance increases with increasing doses from 0 kGy (ACC-00 electrode) until 1 kGy for the ACCD and ACCF electrodes. However, the SC cells performance decreased at overdoses of 3 and 6 kGy for both ACCD and ACCF electrodes. The ACCD-01 and ACCF-01 SC cells exhibit the largest CV area than others, translating into the most significant C_{sp} values (Table 4). At the low CV scan rate, the C_{sp} represents peak values because the conducting electrolyte ions have more time to penetrate deeper into available electrode pores and form electric double layers. The trend of increasing, decreasing and exhibition of maximum at 1 kGy of the C_{sp} values in CV analysis follows the EIS analysis.

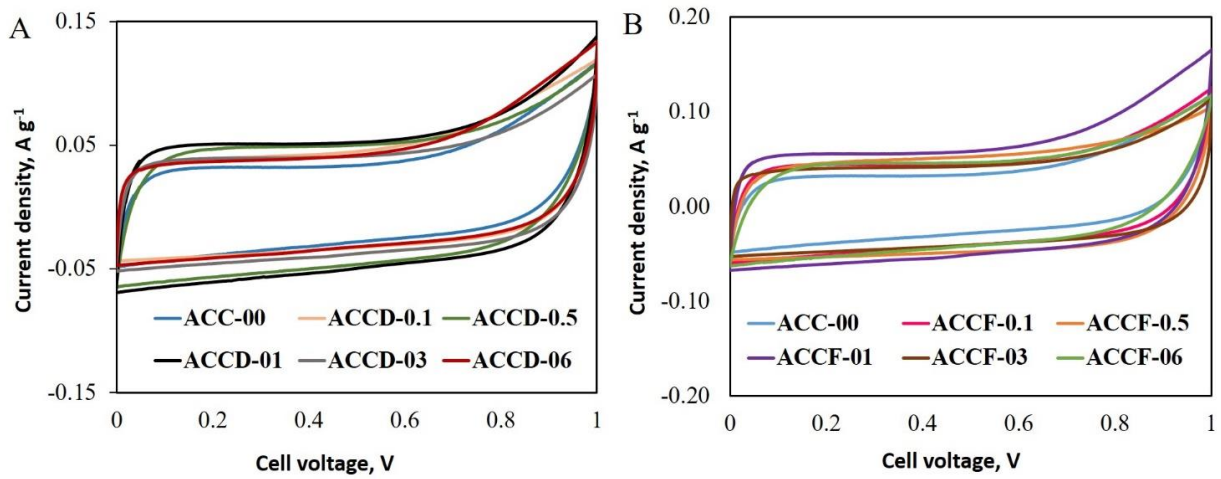

Figure 8. *Cyclic voltammograms at 1 mV s^{-1} for SC cells made from: (A) direct radiation modality, ACCD samples, and (B) filtered radiation modality, ACCF samples, at different irradiation doses. The SC made from non-radiated ACC-00 are shown on both sides for reference*

Galvanostatic charge-discharge (GCD)

The current density is an essential factor for SCs as it directly characterizes capacitive behavior. The GCD curves of the SC cells are shown in Figures 9(A) and 9(B) at a current density of 0.7 A g^{-1}. The curves show a triangular shape and exhibit small IR drops (the voltage drop due to inner resistance at the initial stage of the discharge process), which are typical for carbon-based materials. The charge-discharge capacity that determines the performance of the SC cells were calculated using equation (6), (7) and (8) for C_{sp}, P and E parameters, respectively. The upward trend (C_{sp}, P and E values) with irradiation doses is similar to previous EIS and CV analysis; the values peaked at 1 kGy and decreased for 3 and 6 kGy (Table 4). The relationship between E and P of the SC cells (Figures 9(C) and 9(D)) shows the significant overall performance gain of SC cells made from ACCD-01 and ACCF-01.

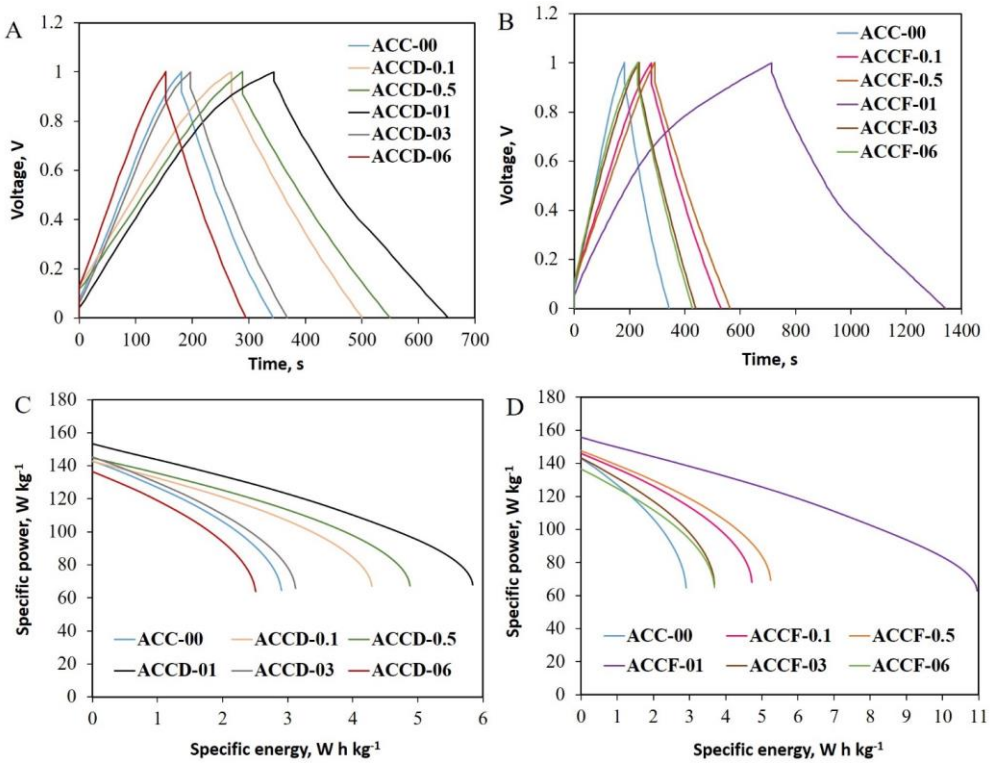

Figure 9. *GCD curves at 0.7 A g^{-1} for SC cells made from: (A) ACCD and (B) ACCF electrodes, where ACC-00 are present on both sides for comparison; (C) and (D) their respective Ragone plots*

Conclusions

Based on the results obtained in this study, the electrochemical performance gain by ACCD and ACCF SC cells can be attributed to increasing lattice defects, mesopores improvement over micropores (S_{meso}/S_{micro}) and an increasing degree of disorder (I_D/I_G). In visual identification through N_2 adsorption-desorption isotherm curves and FESEM pictures, it is hard to identify the radiation effect because it is the intrinsic nature of carbon structures. However, the radiation effects are elucidated in XRD (the changes in the lattice parameters), Raman (defect parameter), FTIR (reduction of individual functional group bonds) and in the electrochemical analysis. This study indicates that lattice defect modification in the AC is vital, as well as the AC electrode surface area in improving the SC performance. Both ACCD and ACCF electrodes have almost equal S_{BET} as the ACC-00 electrode. However, the SC made from ACCD and ACCF electrodes have better overall performance than SC made from ACC-00. The use of a filter to increase the composition of the secondary electron (as in ACCF) has shown significant improvement in the electrochemical performance (up to 51, 47 and 1.4 % increase in C_{sp}, E and P, respectively, in the GCD analysis) at 1 kGy of optimal exposure dose (ACCF-01 compared to the ACCD-01). The SC made from ACCF-01 has better overall performance than SCs made from other electrodes such as ACCFs, ACCDs and ACC-00. The defect created on the AC lattice is more assertive when deterministic radiation modality (filtered) is used than stochastic radiation modality (direct). It can be concluded that the importance of secondary electrons composition in the radiation field and the optimal dose of 1 kGy have an influential role in this study pretreatment of the ACs.

Acknowledgment: *We acknowledge the grant GUP-2017-045 and the support from CRIM, UKM. The authors also thank Saini Sain for laboratory assistance.*

References

[1] P. A. Owusu, S. Asumadu-Sarkodie, *Cogent Engineering* **3** (2016) 1167990. https://doi.org/10.1080/23311916.2016.1167990

[2] H. Wang, Z. Xu, A. Kohandehghan, Z. Li, K. Cui, X. Tan, T. J. Stephenson, C. K. King'ondu, C. M. B. Holt, B. C. Olsen, J. K. Tak, D. Harfield, A. O. Anyia, D. Mitlin, *ACS Nano* **7** (2013) 5131–5141. https://doi.org/10.1021/nn400731g

[3] B. Zhao, D. Chen, X. Xiong, B. Song, R. Hu, Q. Zhang, B. H. Rainwater, G. H. Waller, D. Zhen, Y. Ding, Y. Chen, C. Qu, D. Dang, C.-P. Wong, M. Liu, *Energy Storage Materials* **7** (2017) 32–39. https://doi.org/10.1016/j.ensm.2016.11.010

[4] B. K. Kim, S. Sy, A. Yu, J. Zhang, *Handbook of Clean Energy Systems*, John Wiley & Sons Ltd, Chichester, UK, 2015, p. 1–25. https://doi.org/10.1002/9781118991978.hces112

[5] A. Burke, H. Zhao, *2015 IEEE 82nd Vehicular Technology Conference (VTC2015-Fall)*, Boston, USA, 2015. p. 1–5. https://doi.org/10.1109/VTCFall.2015.7391093

[6] G. Xiong, P. He, Z. Lyu, T. Chen, B. Huang, L. Chen, T. S. Fisher, *Nature Communications* **9** (2018) 790. https://doi.org/10.1038/s41467-018-03112-3

[7] K. Jung, W. Deng, D. W. Smith, J. P. Ferraris, *Electrochemistry Communications* **23** (2012) 149–152. https://doi.org/10.1016/j.elecom.2012.07.026

[8] C. Li, X. Yang, G. Zhang, *Materials Letters* **161** (2015) 538–541. https://doi.org/10.1016/j.matlet.2015.09.003

[9] H.-J. Choi, S.-M. Jung, J.-M. Seo, D. W. Chang, L. Dai, J.-B. Baek, *Nano Energy* **1** (2012) 534–551. https://doi.org/10.1016/j.nanoen.2012.05.001

[10] H. Shen, E. Liu, X. Xiang, Z. Huang, Y. Tian, Y. Wu, Z. Wu, H. Xie, *Materials Research Bulletin* **47** (2012) 662–666. https://doi.org/10.1016/j.materresbull.2011.12.028

[11] G. A. Snook, P. Kao, A. S. Best, *Journal of Power Sources* **196** (2011) 1–12. https://doi.org/10.1016/j.jpowsour.2010.06.084

[12] H. Xiao, S. Yao, H. Liu, F. Qu, X. Zhang, X. Wu, *Progress in Natural Science: Materials International* **26** (2016) 271–275. https://doi.org/10.1016/j.pnsc.2016.05.007

[13] V. Subramanian, S. C. Hall, P. H. Smith, B. Rambabu, *Solid State Ionics* **175** (2004) 511–515. https://doi.org/10.1016/j.ssi.2004.01.070

[14] D.-Q. Liu, S.-H. Yu, S.-W. Son, S.-K. Joo, *ECS Transactions* **16** (2008) 103–109. https://doi.org/10.1149/1.2985632

[15] K. Liu, Y. Zhang, W. Zhang, H. Zheng, G. Su, *Transactions of Nonferrous Metals Society of China* **17** (2007) 649–653. https://doi.org/10.1016/S1003-6326(07)60150-2

[16] C. Peng, X. Yan, R. Wang, J. Lang, Y. Ou, Q. Xue, *Electrochimica Acta* **87** (2013) 401–408. https://doi.org/10.1016/j.electacta.2012.09.082

[17] J. Mi, X.-R. Wang, R.-J. Fan, W.-H. Qu, W.-C. Li, *Energy & Fuels* **26** (2012) 5321–5329. https://doi.org/10.1021/ef3009234

[18] R. Farma, M. Deraman, I. A. Talib, Awitdrus, R. Omar, M. M. Ishak, E. Taer, N. H. Basri, B. N. M. Dolah, *5th Asian Physics Symposium (APS 2012)*, Bandung, Indonesia, 2012, p. 030006. https://doi.org/10.1063/1.4917095

[19] A. E. Ismanto, S. Wang, F. E. Soetaredjo, S. Ismadji, *Bioresource Technology* **101** (2010) 3534–3540. https://doi.org/10.1016/j.biortech.2009.12.123

[20] V. Subramanian, C. Luo, A. M. Stephan, K. S. Nahm, S. Thomas, B. Wei, *The Journal of Physical Chemistry C* **111** (2007) 7527–7531. https://doi.org/10.1021/jp067009t

[21] D. Prahas, Y. Kartika, N. Indraswati, S. Ismadji, *Chemical Engineering Journal* **140** (2008) 32–42. https://doi.org/10.1016/j.cej.2007.08.032

[22] X. Li, W. Xing, S. Zhuo, J. Zhou, F. Li, S.-Z. Qiao, G.-Q. Lu, *Bioresource Technology* **102** (2011) 1118–1123. https://doi.org/10.1016/j.biortech.2010.08.110

[23] J. Li, Q. Wu, *New Journal of Chemistry* **39** (2015) 3859–3864. https://doi.org/10.1039/C4N

J01853B

[24] K. Charoensook, C.-L. Huang, H.-C. Tai, V. V. K. Lanjapalli, L.-M. Chiang, S. Hosseini, Y.-T. Lin, Y.-Y. Li, *Journal of the Taiwan Institute of Chemical Engineers* **120** (2021) 246–256. https://doi.org/10.1016/j.jtice.2021.02.021

[25] E. Taer, P. Dewi, Sugianto, R. Syech, R. Taslim, Salomo, Y. Susanti, A. Purnama, Apriwandi, Agustino, R. N. Setiadi, *The 1st International Conference And Exhibition On Powder Technology Indonesia (ICePTi) 2017*, Jatinangor, Indonesia, 2017, p. 030026. https://doi.org/10.1063/1.5021219

[26] T. E. Rufford, D. Hulicova-Jurcakova, Z. Zhu, G. Q. Lu, *Electrochemistry Communications* **10** (2008) 1594–1597. https://doi.org/10.1016/j.elecom.2008.08.022

[27] J. Chen, Y. Zhai, H. Chen, C. Li, G. Zeng, D. Pang, P. Lu, *Applied Surface Science* **263** (2012) 247–253. https://doi.org/10.1016/j.apsusc.2012.09.038

[28] J. Chmiola, G. Yushin, Y. Gogotsi, C. Portet, P. Simonand, P. L. Taberna, *Science* **313** (2006) 1760–1763. https://doi.org/10.1126/science.1132195

[29] H. P. S. A. Khalil, H. Ismail, H. D. Rozman, M. N. Ahmad, *European Polymer Journal* **37** (2001) 1037–1045. https://doi.org/10.1016/S0014-3057(00)00199-3

[30] C. Su, M. Tripathi, Q.-B. Yan, Z. Wang, Z. Zhang, C. Hofer, H. Wang, L. Basile, G. Su, M. Dong, J. C. Meyer, J. Kotakoski, J. Kong, J.-C. Idrobo, T. Susi, J. Li, *Science Advances* **5** (2019) eaav2252. https://doi.org/10.1126/sciadv.aav2252

[31] D. Sekulićc, B. Babić, L. Kljajević, J. Stašicć B. Kaluđerović, *Journal of the Serbian Chemical Society* **74** (2009) 1125–1132. https://doi.org/10.2298/JSC0910125S

[32] N. S. Mohd Nor, M. Deraman, R. Omar, Awitdrus, R. Farma, N. H. Basri, B. N. Mohd Dolah, N. F. Mamat, B. Yatim, M. N. Md Daud, *Energy* **79** (2015) 183–194. https://doi.org/10.1016/j.energy.2014.11.002

[33] B. Li, Y. Feng, K. Ding, G. Qian, X. Zhang, J. Zhang, *Carbon* **60** (2013) 186–192. https://doi.org/10.1016/j.carbon.2013.04.012

[34] V. A. Kislenko, S. V. Pavlov, S. A. Kislenko, *Electrochimica Acta* **341** (2020) 136011. https://doi.org/10.1016/j.electacta.2020.136011

[35] C. N. Barnakov, G. P. Khokhlova, A. N. Popova, S. A. Sozinov, Z. R. Ismagilov, *Eurasian Chemico-Technological Journal* **17** (2015) 87. https://doi.org/10.18321/ectj198

[36] T. K. Enock, C. K. King'ondu, A. Pogrebnoi, Y. A. C. Jande, *Materials Today Energy* **5** (2017) 126–137. https://doi.org/10.1016/j.mtener.2017.06.006

[37] M. Beidaghi, W. Chen, C. Wang, *Journal of Power Sources* **196** (2011) 2403–2409. https://doi.org/10.1016/j.jpowsour.2010.09.050

[38] S. R. S. Prabaharan, R. Vimala, Z. Zainal, *Journal of Power Sources* **161** (2006) 730–736. https://doi.org/10.1016/j.jpowsour.2006.03.074

[39] X. Geng, L. Li, M. Zhang, B. An, X. Zhu, *Journal of Environmental Sciences* **25** (2013) S110–S117. https://doi.org/10.1016/S1001-0742(14)60638-0

[40] T. K. Manimekalai, G. Tamilarasan, N. Sivakumar, S. Periyasamy, *International Journal of ChemTech Research* **8** (2015) 225–240.

[41] H. P. S. A. Khalil, M. Jawaid, P. Firoozian, U. Rashid, A. Islam, H. M. Akil, *Journal of Biobased Materials and Bioenergy* **7** (2013) 708–714. https://doi.org/10.1166/jbmb.2013.1379

[42] S. J. Gregg, K. S. W. Sing, *Adsorption, Surface Area and Porosity*, Academic Press, London, 1982. https://doi.org/10.1002/bbpc.19820861019

[43] P. González-García, T. A. Centeno, E. Urones-Garrote, D. Ávila-Brande, L. C. Otero-Díaz, *Applied Surface Science* **265** (2013) 731–737. https://doi.org/10.1016/j.apsusc.2012.11.092

[44] D. Ma, G. Wu, J. Wan, F. Ma, W. Geng, S. Song, *RSC Advances* **5** (2015) 107785–107792. https://doi.org/10.1039/C5RA24401C

[45] A. Sarkar, K. Dasgupta, P. Barat, P. Mukherjee, D. Sathiyamoorthy, *International Journal of*

Modern Physics B **22** (2008) 865-875. https://doi.org/10.1142/S0217979208038119
[46] T. Brousse, M. Toupin, R. Dugas, L. Athouël, O. Crosnier, D. Bélanger, *Journal of The Electrochemical Society* **153** (2006) A2171. https://doi.org/10.1149/1.2352197
[47] B. Manoj, A. G. Kunjomana, *International Conference on Materials Science and Technology (ICMST 2012),* Kerala, India, 2012, 012096. https://doi.org/10.1088/1757-899X/73/1/012096
[48] R. Hendriansyah, T. Prakoso, P. Widiatmoko, I. Nurdin, H. Devianto, *MATEC Web of Conferences* **156** (2018) 03018. https://doi.org/10.1051/matecconf/201815603018
[49] D. Qu, *Journal of Power Sources* **109** (2002) 403–411. https://doi.org/10.1016/S0378-7753(02)00108-8
[50] J.-S. Roh, *Carbon Letters* **9** (2008) 127–130. https://doi.org/10.5714/CL.2008.9.2.127
[51] B. Senthilkumar, Z. Khan, S. Park, K. Kim, H. Ko, Y. Kim, *Journal of Materials Chemistry A* **3** (2015) 21553–21561. https://doi.org/10.1039/C5TA04737D
[52] M. A. Pimenta, G. Dresselhaus, M. S. Dresselhaus, L. G. Cançado, A. Jorio, R. Saito, *Physical Chemistry Chemical Physics* **9** (2007) 1276–1290. https://doi.org/10.1039/B613962K
[53] V. T. Nguyen, H. D. Le, V. C. Nguyen, T. T. T. Ngo, D. Q. Le, X. N. Nguyen, N. M. Phan, *Advances in Natural Sciences: Nanoscience and Nanotechnology* **4** (2013) 035012. https://doi.org/10.1088/2043-6262/4/3/035012
[54] J. Shi, D. Xing, J. Lia, *Energy Procedia* **16** (2012) 758–762. https://doi.org/10.1016/j.egypro.2012.01.122
[55] J. H. Hubel, S. M. Seltzer, **23** (1995) 203. https://nvlpubs.nist.gov/nistpubs/Legacy/IR/nistir5632.pdf
[56] A.-N. A. El-Hendawy, *Journal of Analytical and Applied Pyrolysis* **75** (2006) 159–166. https://doi.org/10.1016/j.jaap.2005.05.004
[57] A. J. R. Rennie, V. L. Martins, R. M. Smith, P. J. Hall, *Scientific Reports* **6** (2016) 22062. https://doi.org/10.1038/srep22062
[58] F. Yang, X. Liu, R. Mi, L. Yuan, X. Yang, M. Zhong, Z. Fu, C. Wang, Y. Tang, *Nanomaterials* **8** (2018) 533. https://doi.org/10.3390/nano8070533
[59] S. Qu, J. Wan, C. Dai, T. Jin, F. Ma, *Journal of Alloys and Compounds* **751** (2018) 107–116. https://doi.org/10.1016/j.jallcom.2018.04.123